

The VDAC Technique: A Variational Method for Detecting and Characterizing Convective Vortices in Multiple-Doppler Radar Data

COREY K. POTVIN AND ALAN SHAPIRO

School of Meteorology, and Center for Analysis and Prediction of Storms, University of Oklahoma, Norman, Oklahoma

MICHAEL I. BIGGERSTAFF

School of Meteorology, University of Oklahoma, Norman, Oklahoma

JOSHUA M. WURMAN

Center for Severe Weather Research, Boulder, Colorado

(Manuscript received 24 September 2010, in final form 21 January 2011)

ABSTRACT

The vortex detection and characterization (VDAC) technique is designed to identify tornadoes, mesocyclones, and other convective vortices in multiple-Doppler radar data and retrieve their size, strength, and translational velocity. The technique consists of fitting radial wind data from two or more radars to a simple analytical model of a vortex and its near environment. The model combines a uniform flow, linear shear flow, linear divergence flow (all of which comprise a broad-scale flow), and modified combined Rankine vortex. The vortex and its environmental flow are allowed to translate. A cost function accounting for the discrepancy between the model and observed radial winds is evaluated over space and time so that observations can be used at the actual times and locations they were acquired. The model parameters are determined by minimizing this cost function.

Tests of the technique using analytically generated, numerically simulated, and one observed tornadic wind field were presented by Potvin et al. in an earlier study. In the present study, an improved version of the technique is applied to additional real radar observations of tornadoes and other substorm-scale vortices. The technique exhibits skill in detecting such vortices and characterizing their size and strength. Single-Doppler experiments suggest that the technique may reliably detect and characterize larger (>1 -km diameter) vortices even in the absence of overlapping radar coverage.

1. Introduction

The severe thunderstorm and tornado warning process becomes particularly challenging when forecasters do not have time to thoroughly interrogate all available radar data or when observations and model forecasts are only marginally supportive of severe weather prior to its onset. The former scenario is common during severe weather outbreaks, especially if the county warning area (CWA) exists within several Doppler radar domains. Lowered forecaster situational awareness in the latter scenario likely explains the documented increase in

zero-lead-time warnings on the first tornado of the day, particularly if it is the only tornado in/near the CWA that day (Brotzge and Erickson 2010). Radar-based detection algorithms become particularly important in these cases, serving to alert forecasters to important features they may otherwise have missed.

Since the implementation of the Weather Surveillance Radar 1988-Doppler (WSR-88D) network, several algorithms have been developed to aid forecasters in real-time identification of intense convective vortices. These include the tornado vortex signature (TVS) algorithm (Crum and Alberty 1993), the National Severe Storms Laboratory (NSSL) mesocyclone detection algorithm (MDA; Stumpf et al. 1998), and the NSSL tornado detection algorithm (TDA; Mitchell et al. 1998). Unfortunately, since these techniques rely upon thresholds of gate-to-gate shear, they are particularly sensitive to

Corresponding author address: Corey K. Potvin, National Severe Storms Laboratory, Forecast Research and Development Division, Room 4355, 120 David L. Boren Blvd., Norman, OK 73072.
E-mail: corey.potvin@noaa.gov

noise in the velocity data and to azimuthal offset of vortices from the radar beam. This results in a sharp trade-off between the false alarm rate (FAR) and probability of detection (POD).

The velocity track display (VTD) technique and its variants (Lee et al. 1994; Roux and Marks 1996; Lee et al. 1999; Liou et al. 2006) fit radial velocity data to a vortex model in order to recover key characteristics of the vortex flow. This approach is less sensitive to noisy velocity data than are shear-based techniques. However, the VTD techniques are not designed to retrieve the vortex center, which instead must be predetermined using another method. This makes the retrieval of the remaining vortex parameters particularly sensitive to errors in the specified vortex center when the vortex being retrieved is small relative to the observational resolution.

The vortex detection and characterization (VDAC) technique described herein also adopts a vortex-fitting approach. More specifically, radial wind observations from two or more close-proximity Doppler radars with overlapping domains are fit to an analytical low-order model of a vortex and its near environment. This capability distinguishes our approach from traditional dual-Doppler analysis methods, which do not constrain the retrieved wind field with a spatial vortex model and thus are not designed to retrieve vortex characteristics. The ability of the technique to use data from multiple radars makes it comparable to the dual-Doppler extended ground-based VTD (EGBVTD; Liou et al. 2006). However, the model parameters in the VDAC method include the vortex center, making a priori knowledge of the location of the vortex unnecessary. This allows the technique to function as both a vortex detection algorithm and a vortex characterization algorithm. The VDAC technique is designed primarily for use in Collaborative Adaptive Sensing of the Atmosphere (CASA; McLaughlin et al. 2005; Brotzge et al. 2007) and CASA-like radar networks, whose high observational resolution and overlapping coverage should permit more accurate detection and characterization of tornado- and mesocyclone-scale vortices than is possible with the WSR-88D network. However, it will be shown that the technique may reliably detect and characterize vortices >1 km in diameter even when velocity data from only one radar are available.

A complete description of the original VDAC methodology, as well as tests of the technique using analytically generated, numerically simulated and one observed tornadic wind field, was presented in Potvin et al. (2009). In the current study, important improvements to the technique as well as tests with additional radar observations of convective vortices are shown. The rest of the

paper is organized as follows. The updated low-order model is described in section 2. The retrieval methodology, including the cost function computation and the selection of analysis domains, is described in section 3. Section 4 describes the new detection criteria. In sections 5–7, the technique is tested using Shared Mobile Atmospheric Research and Teaching (SMART; Biggerstaff et al. 2005) radar observations of the 30 May 2004 Geary, Oklahoma, tornadic supercell; Doppler-on-Wheels (DOW; Wurman et al. 1997) observations of a tornado that occurred near Argonia, Kansas, on 5 June 2001; and CASA observations of the 14 May 2009 Anadarko, Oklahoma, tornado. The ability of the technique to detect and characterize vortices >1 km in diameter is explored in section 8. A summary and conclusions follow in section 9.

2. Description of low-order model

The low-order model to which the Doppler velocity data are fit comprises four idealized flow fields: a uniform flow, linear shear flow, and linear divergence flow (together constituting the “broad-scale” flow), and a modified combined Rankine vortex (MCRV; e.g., Hughes 1952; Brown et al. 2002), which is a combination of two axisymmetric flow fields. The interior (or “core”) of the MCRV is a solid body vortex. Outside of the MCRV core, the radial and tangential vortex winds decrease as a power of distance from the vortex center. The use of the MCRV model is supported qualitatively by high-resolution mobile radar observations of tornadoes (Wurman and Gill 2000; Bluestein et al. 2003; Lee and Wurman 2005). Although tornadic wind fields can severely violate the MCRV model within/near suction vortices (e.g., Wurman 2002), the larger-scale structure of multiple-vortex tornadoes can still be reasonably captured by the model. In cases where the vortex-scale wind field departs significantly from the MCRV model, as in tornadoes that are elliptically shaped (e.g., Bluestein et al. 2003) because of the translation of the vortex (Lewellen et al. 2000) or the presence of a deformation zone (e.g., along a gust front), the broad-scale model parameters can account for some of the asymmetry in the vortex wind field, thereby facilitating retrieval of the axisymmetric portion of the vortex.

The vortex and the horizontal broad-scale fields are allowed to translate, allowing radar data to be used at their actual locations and times of acquisition and thus bypassing the need for temporal interpolation, moving reference frames, or other ad hoc procedures. A total of 19 parameters (Table 1) characterize the wind field in the low-order model. These parameters are considered constant over a single 4D retrieval domain; that is, the

TABLE 1. Low-order model parameters.

Parameters	Description
a, d	x and y components of uniform flow velocity (m s^{-1})
b, e	x and y components of horizontal shear (s^{-1})
c, f	x and y components of horizontal divergence (s^{-1})
g, h	x and y components of vertical shear (s^{-1})
R	Vortex radius of maximum wind (m)
V_R, V_T	Maximum vortex radial and tangential winds (m s^{-1})
x_0, y_0	Vortex center location at $t = 0$ (m)
u_b, v_b	Broad-scale translational velocity components (m s^{-1})
u_v, v_v	Vortex translational velocity components (m s^{-1})
α, β	Decay exponents for vortex radial and tangential winds

low-order model does not make provision for flow evolution. For the typical observational periods (<30 s) for which the technique is designed, however, this is not expected to be a significant limitation.

The horizontal components V_x and V_y of the broad-scale portion of the model are given by

$$\begin{aligned} V_x &= a + b(y - v_b t) + c(x - u_b t) + gz, \\ V_y &= d + e(x - u_b t) + f(y - v_b t) + hz. \end{aligned} \quad (1)$$

The vertical shear parameters g and h were not included in the original low-order model used in Potvin et al. (2009). They have been added to improve the retrieval of the broad-scale flow in cases where the horizontal winds vary substantially with height over the retrieval domain. Since quasi-horizontal retrieval domains were

used in all of the experiments presented below (the reason for this is given in section 3a), the vertical shear was generally not well observed, and so significant errors occurred in g and h . However, since these errors resulted from solution nonuniqueness rather than from violation of the low-order model, they did not degrade the retrieval of the remaining parameters.

The vortex azimuthal velocity field v_θ and vortex radial velocity field v_r are given by

$$v_\theta = \begin{cases} \frac{r}{R} V_T, & r < R, \\ \frac{R^\alpha}{r^\alpha} V_T, & r \geq R, \end{cases} \quad v_r = \begin{cases} \frac{r}{R} V_R, & r < R, \\ \frac{R^\beta}{r^\beta} V_R, & r \geq R, \end{cases} \quad (2)$$

where

$$r = \sqrt{(x - x_0 - u_v t)^2 + (y - y_0 - v_v t)^2} \quad (3)$$

is the distance of a given (x, y) coordinate from the center of the vortex (located at x_0, y_0 at the analysis time $t = 0$) at time t . It can be noted that the broad-scale wind equations implicitly make provision for a large (relative to the analysis domain) vortex since the Cartesian representation of a solid body vortex is $u = -\Omega y, v = \Omega x$, where Ω is the (constant) vortex angular velocity. Casting the MCRV equations into Cartesian coordinates, adding the linear flow fields, and taking the radial projection (with respect to a radar) of the result yields the model Doppler radar velocity V_r^{mod} :

$$\begin{aligned} V_r^{\text{mod}} &= \cos\phi_n \sin\theta_n \left[a + b(y - v_b t) + c(x - u_b t) + gz + \frac{V_R}{R}(x - x_0 - u_v t) - \frac{V_T}{R}(y - y_0 - v_v t) \right] \\ &\quad + \cos\phi_n \cos\theta_n \left[d + e(x - u_b t) + f(y - v_b t) + hz + \frac{V_R}{R}(y - y_0 - v_v t) + \frac{V_T}{R}(x - x_0 - u_v t) \right] \quad r < R, \\ &= \cos\phi_n \sin\theta_n \left[a + b(y - v_b t) + c(x - u_b t) + gz + \frac{R^\beta V_R (x - x_0 - u_v t)}{r^{\beta+1}} - \frac{R^\alpha V_T (y - y_0 - v_v t)}{r^{\alpha+1}} \right] \\ &\quad + \cos\phi_n \cos\theta_n \left[d + e(x - u_b t) + f(y - v_b t) + hz + \frac{R^\beta V_R (y - y_0 - v_v t)}{r^{\beta+1}} + \frac{R^\alpha V_T (x - x_0 - u_v t)}{r^{\alpha+1}} \right] \quad r \geq R, \end{aligned} \quad (4)$$

where θ_n and ϕ_n are the azimuth and elevation angles, respectively, of the n th radar (θ_n is measured clockwise from the north). The contributions of the vertical wind component and falling hydrometeors to Doppler velocity observations are neglected since operational radars typically scan at relatively shallow elevation angles. The complete derivation of the model radial wind is given in Potvin et al. (2009).

3. Retrieval methodology

a. Cost function computation and minimization

Within each analysis domain, a cost function J sums the (squared) discrepancies between the observed and model radial wind fields over the spatiotemporal domains of N radars scanning in range r , azimuth θ , and elevation angle ϕ :

$$J \equiv \sum_{n=1}^N \sum_{m=1}^M \sum_{\phi} \sum_{\theta} \sum_r \left(\frac{r_n}{r_{\text{mean}}} \right)^2 (V_r^{\text{obs}} - V_r^{\text{mod}})^2, \quad (5)$$

where M is the total number of full volume scans (temporal sum), r_n is the radial distance of an observation point from the n th radar, and r_{mean} is the mean r_n over the N radars within the analysis domain. A range-weighting factor r_n^2/r_{mean}^2 accounts for the expansion of radar resolution volumes (and the corresponding regions over which observations are valid) with distance from the radar. The cost function J provides a useful way to quantitatively compare the quality of retrievals for different experiments and, when appropriately normalized, can be used to calculate the mean model error per radar grid point.

Although the technique can use data from multiple elevation angles and volume scans, it is generally better to use only one plan position indicator (PPI) scan (per radar) at a time. This minimizes violation of the low-order model by vortices that vary significantly in height or time. For example, in the case of an intense vortex developing in an up-down or down-up fashion, the V_T retrieved using radar data collected through the depth of the vortex would likely be less than that retrieved using data from a single pair of PPI scans through the stronger layer of the vortex. This could prevent the vortex from being detected (the detection criteria are discussed in section 4).

The cost function J is minimized to retrieve the set of parameter values producing the least squares error in the model wind (best fit between model and observed winds). In view of (5) and the locations of the model parameters in (4), our minimization problem is highly nonlinear. Conjugate gradient minimization methods have proven useful for such problems. This study uses the Polak-Ribiere method (Polak and Ribiere 1969), a robust and efficient variant of the Fletcher and Reeves (1964) algorithm. In both methods, the search direction is reset to that of steepest descent (with all previous direction and gradient information being discarded) every p iterations, where p is the number of model parameters.

As with other minimization techniques, multiple minima in J can prevent the desired minimum (which in our problem may not be the global minimum) from being reached. Multiple minima in the current application can result from the intrinsic nonlinearity of the problem, as well as from areas of missing data and departures of the observed wind field from the model (e.g., multiple proximate vortices). The VDAC technique uses several strategies to mitigate the multiple minima problem, including performing retrievals for a multitude of first-guess vortex centers (section 3b).

b. Selection of analysis domains

Wind field retrievals are conducted within circular analysis domains that are sized according to the typical scales of the vortices sought. Using enough analysis domains to cover the entire dual-Doppler domain, in the absence of a high performance computing cluster, would be too computationally expensive for the technique to be applied in real time. Therefore, retrievals are performed only in regions identified as possibly containing intense vortices. The process by which these regions are selected begins by identifying all pairs of radar gates (in both radar domains) that are located at the same range from the radar and satisfy a set of criteria. Since the typical resolution and quality of velocity data can differ among different CASA-like radar networks, the optimum domain-selection criteria will likewise vary. However, in all of the experiments described herein, the following set of criteria was successful: 1) the azimuthal distance between the two gates is <1 km; 2) the radial velocity difference or the azimuthal shear of radial velocity calculated between the two radar gates exceeds a prescribed threshold; 3) radial wind speed and (optionally) reflectivity exceed prescribed thresholds within 3 km of the centroid of the gate pair; 4) at least 75% of the radial velocity magnitudes within 3 km of each gate exceed 1 m s^{-1} ; and 5) $<20\%$ of the velocity data are missing within both 500 and 1000 m of each of the gates.

Criterion 1 is designed to restrict the vortex retrievals/detections to smaller-scale vortices such as tornadoes and mesocyclones. Criteria 2 and 3 are intended to filter vortices that are too weak to be operationally significant. (Since the purpose of these criteria is to reduce computational time, the use of velocity-based thresholds here does not imply that the VDAC technique is as sensitive to noise and azimuthal offset of vortices from the radar beam as are techniques that rely on gate-to-gate shear thresholds. In fact, an FAR of zero is obtained in all of the experiments presented below despite the majority of retrieval domains being void of intense vortices, suggesting that the domain-selection criteria can be made sufficiently conservative to preserve a high probability of detection without incurring a large number of false alarms.) The reflectivity threshold in criterion 3 reduces the number of retrievals performed outside of convective storms. Criterion 4 is designed to reduce the false alarm rate in cases where ground clutter filtering has introduced significant noise to the radial velocity estimates. Criterion 5 was motivated by experiments (not shown) in which velocity data gaps produced spurious minima in J . For each pair of radar gates satisfying the domain-selection criteria, the centroid

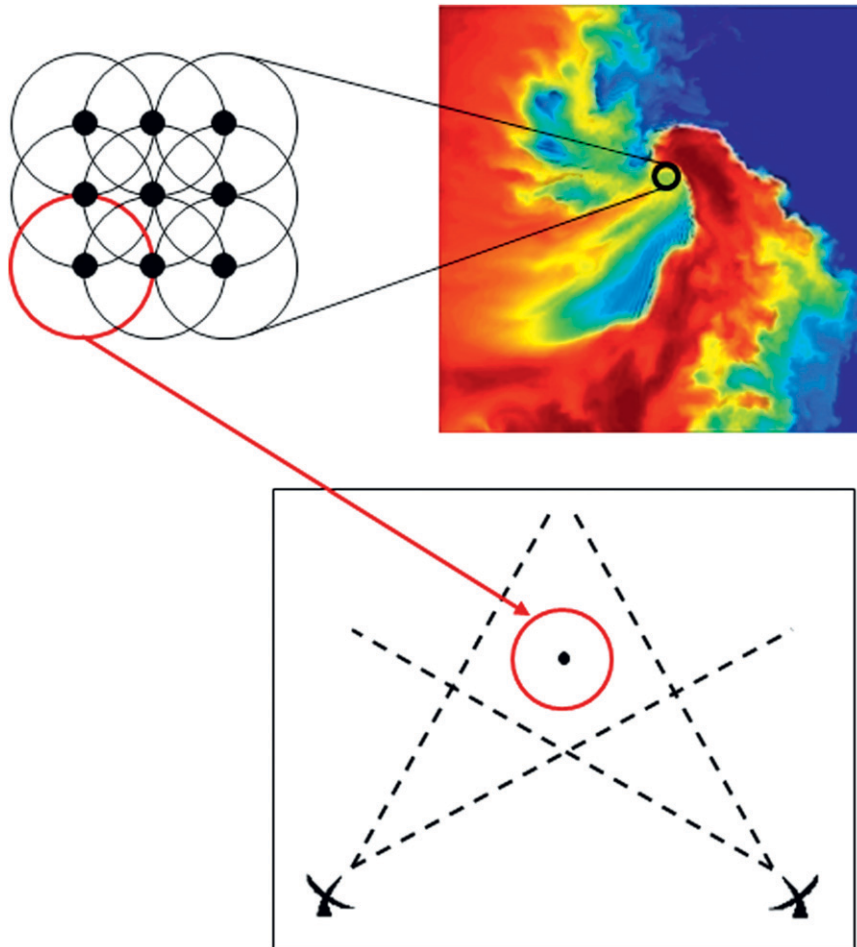


FIG. 1. Schematic illustrating the procedure for selecting the wind retrieval domains. The algorithm searches for regions within the multiple-Doppler radar domain that satisfy prescribed radial velocity and reflectivity criteria. Within each identified region, retrievals are performed over a grid of circular domains whose centers serve as the first guesses for the vortex location(s).

of the two gates is stored. Since vortices always exhibit azimuthal shear signatures in the velocity fields of both radars, all centroids which are located within 2 km of another centroid in the other radar's domain are retained. All such points are then spatially grouped into clusters (since there may be multiple proximate points associated with the same vortex) whose centroids are calculated and stored. Each centroid corresponds to the center of a region over which the retrieval technique will be applied. A horizontal grid of nine first guesses for the vortex center (each serving as the center of an analysis domain over which the retrieval is applied) is subsequently calculated and input to the retrieval routine (Fig. 1). The spacing between the vortex center first guesses is 500 m in both directions. As mentioned above, the use of multiple first guesses for the vortex center makes provision for the presence of multiple vortices or of minima in J that are

not associated with vortices. The initial analysis domain radius was set to 2 km in the experiments below unless stated otherwise.

c. Four-step retrieval procedure

Unfortunately, the global minimum in J does not always correspond to the desired solution in our problem. One situation in which this can occur is when a tornado or other intense, small-scale vortex is embedded within a larger vortex or vortex-like circulation, such as a mesocyclone. In such cases, the larger circulation, by virtue of its larger "footprint," may fit the low-order model better than the smaller vortex, thus preventing the latter from being detected. To address this problem, the minimization procedure was initially split into two steps. In step 1, the vortex model parameters are fixed at zero (except for R since this would introduce a "division

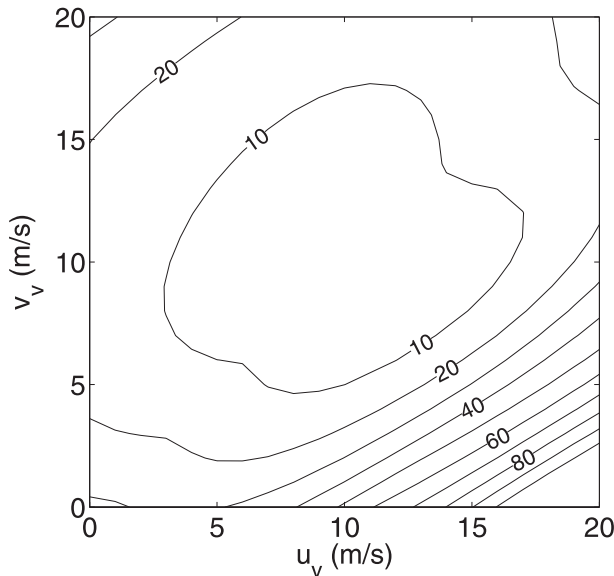


FIG. 2. Values of $J(u_v, v_v)$ ($10^6 \text{ m}^2 \text{ s}^{-2}$) for an analytical vortex with true $(u_v, v_v) = 10 \text{ m s}^{-1}$. Remaining parameters are set to their true values.

by zero" computational issue), and the broad-scale parameters are retrieved. In step 2, the radial components of the wind field retrieved in step 1 are subtracted from the observed radial wind fields, and the retrieval is then repeated on the residual wind field. Since the flow retrieved in step 1 (and subtracted in step 2) is more representative of the broad-scale flow than of the tornadic flow, the tornadic component of the original flow dominates the residual field to be retrieved in step 2, thus improving the vortex retrieval and increasing the probability of detection.

The retrieval procedure has recently been expanded from two to four steps to allow the location and size of the analysis domain to be adjusted according to a preliminary vortex retrieval. This modification was motivated by the fact that, given any analysis domain size that is large enough to encompass most vortices of the type(s) being sought (e.g., tornadoes), the analysis domain will occasionally be much larger than the particular vortex being retrieved. In such cases, a smaller analysis domain is desirable since it allows the vortex to be more salient in the wind field. This is particularly true when the wind field is too complex for the broad-scale parameters to adequately capture the nonvortex flow (or, in the case of an embedded vortex, all of the parent vortex flow) over the initially larger domain.

The first two steps of the new procedure are the same as described above. At the end of step 2, if the retrieved $|V_T|$ exceeds a threshold value, the retrieval proceeds to step 3; otherwise, the retrieval terminates and no vortex

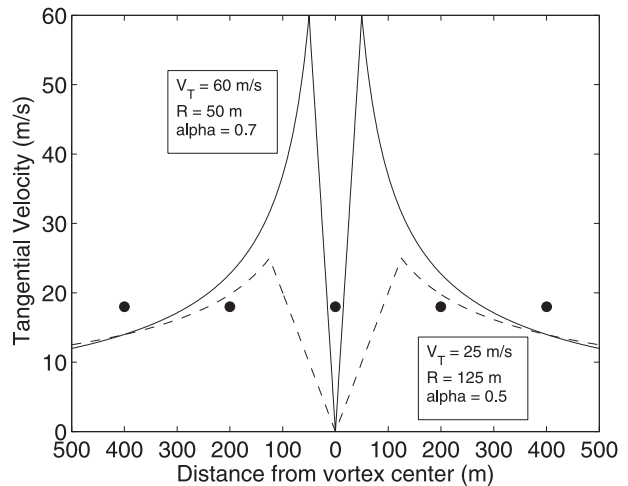


FIG. 3. Tangential velocity profiles for two very different MCRVs. The black dots represent the centers of hypothetical radar probe volumes separated by 200 m. The Doppler velocity fields for these two MCRVs would be very similar for certain probe volume dimensions.

detection is made. Steps 3 and 4 are identical to steps 1 and 2 except the analysis domain is modified according to the size and location of the vortex retrieved in step 2. The new analysis domain is centered on the retrieved vortex location valid midway through the period over which the retrieval is performed, and resized such that the distance between its edge and the nearest point on the retrieved vortex core at the end of the retrieval period is 500 m. The analysis domain used in steps 3 and 4 is thus designed to be as small as possible without excessively truncating the outer vortex winds. If the modified analysis domain would be larger than the default domain, the modified analysis domain radius is set to the default domain radius.

The addition of steps 3 and 4 to the retrieval procedure was particularly beneficial in our experiments in which one vortex was embedded within a parent vortex. In those cases, the vortex retrieved in step 2 tended to better represent the sum of the two vortices than the smaller vortex, whereas the vortex retrieved in step 4 more accurately described the smaller vortex itself.

If the V_T retrieved in step 4 exceeds a threshold value V_{det} , then a set of detection criteria (described in section 4) is used to determine whether an intense vortex has been detected. Otherwise, no information is output and the retrieval procedure restarts at the next first-guess vortex center.

d. Special treatment of vortex translation and position parameters

The vortex translation parameters are often the most difficult vortex parameters to retrieve. If the distance

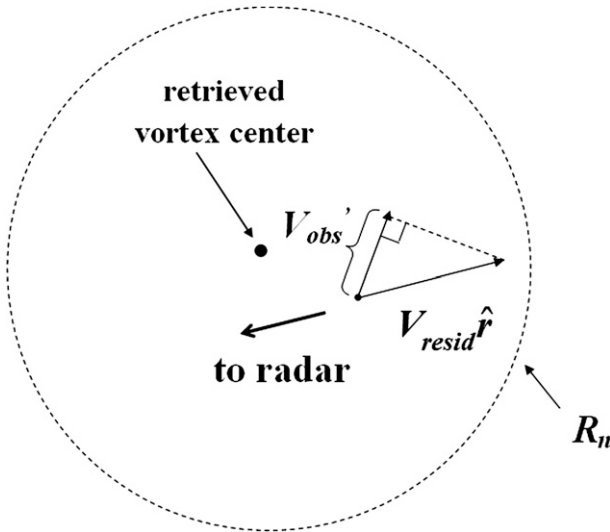


FIG. 4. Computation of V_{obs} , the tangential (relative to the vortex tangential wind) component of a residual radial velocity observation vector \mathbf{V}_{obs} . The retrieved radius of $n \text{ m s}^{-1}$ vortex tangential wind is denoted R_n .

traveled by the vortex during the period between the two radar scans used in the retrieval is small relative to the observational resolution, the intrinsic uncertainty in the vortex center creates a large flat region around the global minimum in $J(u_v, v_v)$ (Fig. 2). Flat regions in J are problematic since they are more likely to contain local minima (common causes of which were listed above), thereby making the retrieval more sensitive to the first guess.

Significant errors in (u_v, v_v) can also occur when multiple regions of azimuthal radial wind shear (including one or more vortices) exist within the analysis domain. In these cases, the retrieved vortex locations valid at the times of each radar scan may in reality correspond to two different features (two different vortices or one vortex and one shear zone). This can result in large errors in (u_v, v_v) and, if the feature “detected” in the first radar scan is not the vortex “detected” in the second radar scan, large errors can also result in (x_0, y_0) . The larger the errors in the first-guess vortex location and translation velocity, the more likely the technique is to mistakenly identify two separate shear features as a single vortex.

To improve the retrieval of the vortex translation and location parameters, particularly in the situation just described, a series of steps is taken to obtain better first guesses for (u_v, v_v) and (x_0, y_0) . Before the wind retrieval is performed, the Gal-Chen (1982) advection retrieval method is applied to the reflectivity field within a circular domain (radius = 10 km) centered on the original analysis domain. Reflectivity data from the current and immediately previous scans of the nearest radar are used; the elevation angle is the same as that used in the wind retrieval. The retrieved reflectivity pattern translational velocity is then used as the first guess for the vortex translational velocity in step 2 of the retrieval procedure. At the end of step 2, J is calculated on a 4D grid of $u_v, v_v, x_0,$ and y_0 values centered on the retrieved solution. The set of $u_v, v_v, x_0,$ and y_0 values with the smallest J is used as the first guess for these parameters in retrieval step 4. This improved first guess increases the probability of the minimization procedure converging to the desired solution.

4. Detection criteria

One of the biggest challenges to developing appropriate detection criteria for this technique was the vortex parameter nonuniqueness problem described in Potvin et al. (2009). In cases where the actual vortex core is small relative to the observational resolution, the combination of the limited observational resolution and ellipticity (flatness) in J owing to the mathematical nature of the MCRV model can create numerous local minima. In particular, this problem frequently results in either significant underestimation of R and overestimation of V_T or significant overestimation of R and underestimation of V_T . This is because, on the scale of the observational resolution, a strong, narrow (poorly resolved) vortex can resemble a weaker, wider (well resolved) vortex and vice versa (Fig. 3). Categorically using the retrieved vortex parameters to distinguish between intense and weak vortices could therefore lead to unacceptable FAR and POD values.

The approach we have adopted instead is to use retrieved vortex characteristics that are verified by the

TABLE 2. Means of retrieved vortex characteristics for each set of 30 May 2004 retrievals from SMART-Radar data. Sample sizes appear in parentheses.

Time (UTC)	Distance from ensemble mean vortex center (m)	Movement (m s^{-1})	Heading ($^\circ$ clockwise from east)	V_T (m s^{-1})	V_T^{res} (m s^{-1})	V_R (m s^{-1})	R (m)	R_{20} (m)	α
0022 (4)	78	29	-33	28	21	-20	393	555	1.4
0027 (17)	81	9	-46	40	20	1	223	519	0.8
0033 (18)	80	15	28	62	33	-13	369	845	1.4
0038 (9)	133	11	-70	50	20	1	332	684	1.3
0052 (29)	90	8	31	73	36	0	264	986	1.0

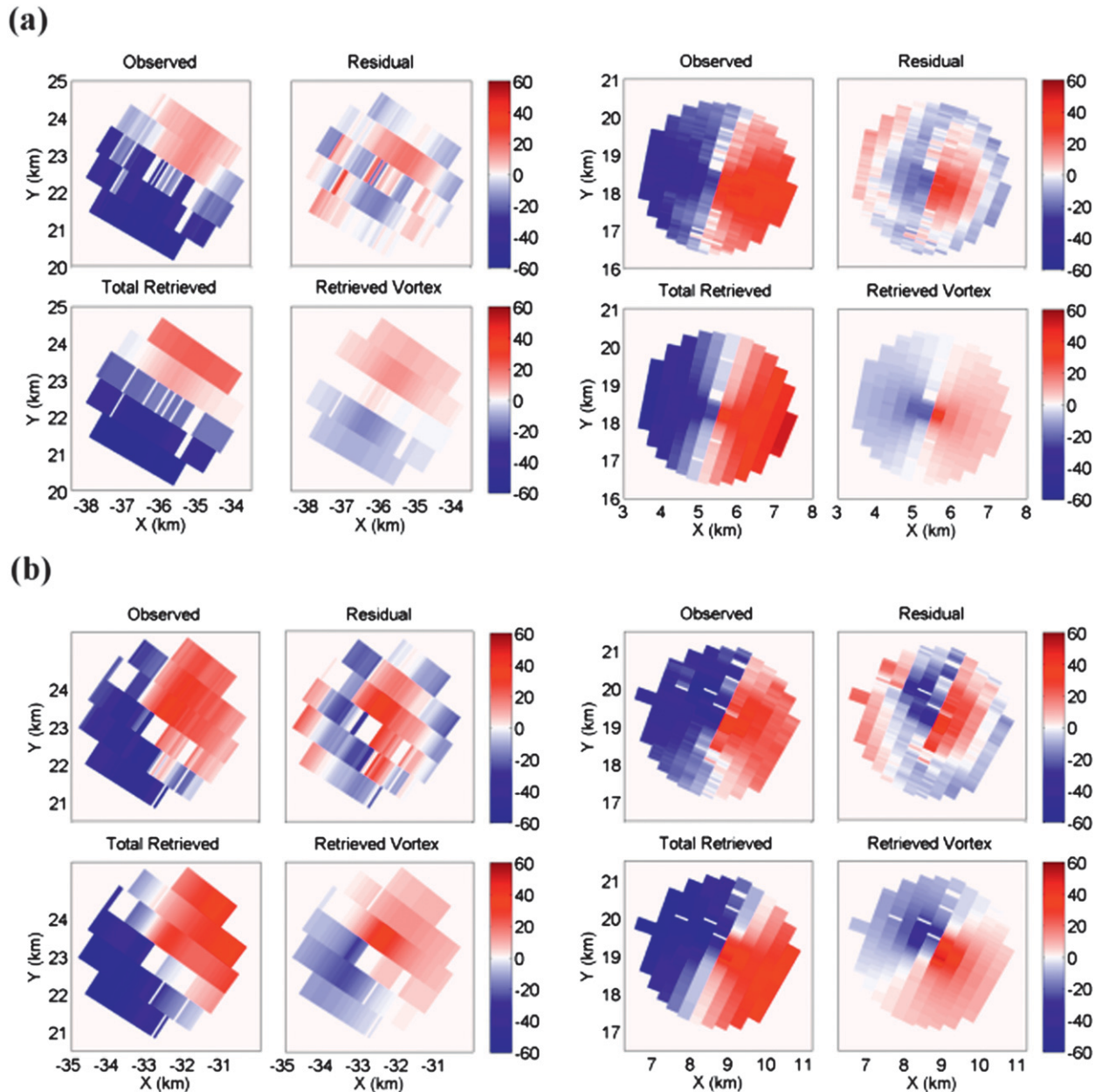


FIG. 5. Observed, residual (observed minus retrieved broad-scale), retrieved vortex, and retrieved total radial velocity fields for (left) SR1 and (right) SR2 at (a) 0027 and (b) 0033 UTC. The axes indicate x and y displacements from the radar.

velocity observations [this is a departure from the detection and characterization methodology used in Potvin et al. (2009)]. If the V_T retrieved in step 4 of the retrieval procedure exceeds a threshold V_{det} , then the outer (i.e., outside the vortex core) radius of $n \text{ m s}^{-1}$ vortex tangential wind R_n is calculated for $n = 10, 15, 20$, and so on. The components of the residual radial winds (calculated in retrieval step 3 and treated as vectors here) tangent to the vortex cylindrical coordinate system V_{obs} are also computed (Fig. 4). For each n , all the V_{obs} values that

exceed n and are located within R_n of the vortex center are identified. If there exists at least one pair of such V_{obs} that are separated from one another by $>90^\circ$ in the azimuthal dimension of the vortex coordinate system, then the values of n and R_n are output to the user (this minimum angular separation criterion helps prevent regions of strong linear shear from being misidentified as strong vortices). If the maximum n meeting these criteria V_T^{tes} is $\geq V_{\text{det}}$, then the vortex is tentatively classified a detection. This approach is inherently conservative since

TABLE 3. Standard deviations of retrieved vortex characteristics for each set of 30 May 2004 retrievals from SMART-Radar data. Asterisked values indicate standard deviations that have been recomputed upon removing an extreme outlier. Sample sizes appear in parentheses.

Time (UTC)	Distance from ensemble mean vortex center (m)	Movement (m s^{-1})	Heading ($^{\circ}$ clockwise from east)	V_T (m s^{-1})	V_T^{res} (m s^{-1})	V_R (m s^{-1})	R (m)	R_{20} (m)	α
0022 (4)	57	5	3	3	3	3	166	133	0.8
0027 (17)	101 (55*)	6	26	6	0	2	44	88	0.2
0033 (18)	55	6	40 (19*)	7	2	6	69	72	0.4
0038 (9)	81	4	27	4	0	1	174	139	0.7
0052 (29)	52	4	98	9	2	2	75	87	0.3

the radial (residual) winds from which the V_{obs} are calculated are themselves only components of the total velocities, meaning that the V_{obs} and thus V_T^{res} will generally be underestimates.

Preliminary detections are subsequently subjected to a set of criteria designed to filter spurious retrievals. If $\geq 25\%$ of the velocity data located within the retrieved outer radius of $V_{\text{det}} \text{ m s}^{-1}$ vortex tangential wind R_{det} are missing, or if the portion of the retrieved vortex with $V_{\theta} > V_{\text{det}}$ extends outside of the analysis domain, the retrieval is rejected since data edges often give rise to local minima. The retrieval is also rejected if the root-mean-square (rms) error (difference between observed and retrieved radial velocity) computed within R_{det} of the retrieved vortex exceeds the rms observed velocity over that same area. This criterion is crucial since retrievals that provide a poor match to the observed wind field can nevertheless be associated with local minima in the typically highly complex cost function surface. This most commonly occurs when one or more contaminated Doppler velocity values create a spurious vortex-like signature in the radial wind field.

In the experiments presented in sections 6 and 7, V_{det} was set to 10 m s^{-1} . In section 5, it was necessary that V_{det} be increased to 20 m s^{-1} to satisfy the detection criterion that the analysis domain contain the outer vortex radius of V_{det} tangential wind. Prior to being implemented in real time, the technique would ideally be modified to automatically increase V_{det} in such cases to prevent particularly intense vortices from being missed.

5. Experiments with SMART radar observations of the 30 May 2004 Geary, Oklahoma, supercell

a. Description of dataset

A supercell that spawned a series of tornadoes across Oklahoma on 30 May 2004 (Bluestein et al. 2007; MacGorman et al. 2008; Kuhlman et al. 2009; Payne et al. 2010) was observed by a pair of SMART radars near Geary and Calumet, Oklahoma. The VDAC technique was tested using base elevation (0.5°) data collected

by the two SMART radars [SMART radar 1 (SR1) and SMART radar 2 (SR2)] at 0022, 0027, 0033, 0038, and 0052 UTC. The data were manually dealiased and noisy or suspect data were manually removed. The range and azimuthal sampling intervals for both radars were approximately 67 m and 1° , respectively, and the half-power beamwidth was about 1.5° . The distance between each of the radars and the analysis domains varied between roughly 20 and 50 km in these tests, yielding azimuthal sampling intervals of between 350 and 850 m. Because of the coordinated radar volume scans, the periods spanned by the observations used in each of the retrievals were relatively short (25–30 s).

An unusually large (1–2-km diameter) surface circulation produced F-2 damage throughout the experimental period (<http://www4.ncdc.noaa.gov/cgi-win/wwcgi.dll?wwevent~ShowEvent~551065>). Several smaller vortices (≤ 1 -km core diameter) formed and decayed within this larger circulation during the SMART radar observing period. These vortices are indicated in the individual radars' wind fields by regions of enhanced shear and are confirmed by the presence of intense shear and reflectivity holes (or "eyes") in higher-resolution DOW observations of this case (Center for Severe Weather Research 2010). Interestingly, the strongest winds measured by both the SMART radars and the DOWs (which sampled to within 50 m of the ground) occurred outside of these vortices. Since the smaller-scale vortices are not readily visually discernable from the surrounding mesoscale vortex flow, this is a useful test case for our algorithm. Which of the vortices (if any) actually extended to the surface as tornadoes is unknown; however, that question is not important here since the goal of these experiments was to verify that the technique is capable of detecting and characterizing vortices having subtle Doppler velocity signatures.

b. Retrieval results

The detection threshold V_{det} was set to 20 m s^{-1} in these experiments. The domain-selection criteria (section 3b) required that the difference in radial wind speed between the two radar gates exceed 15 m s^{-1} and that

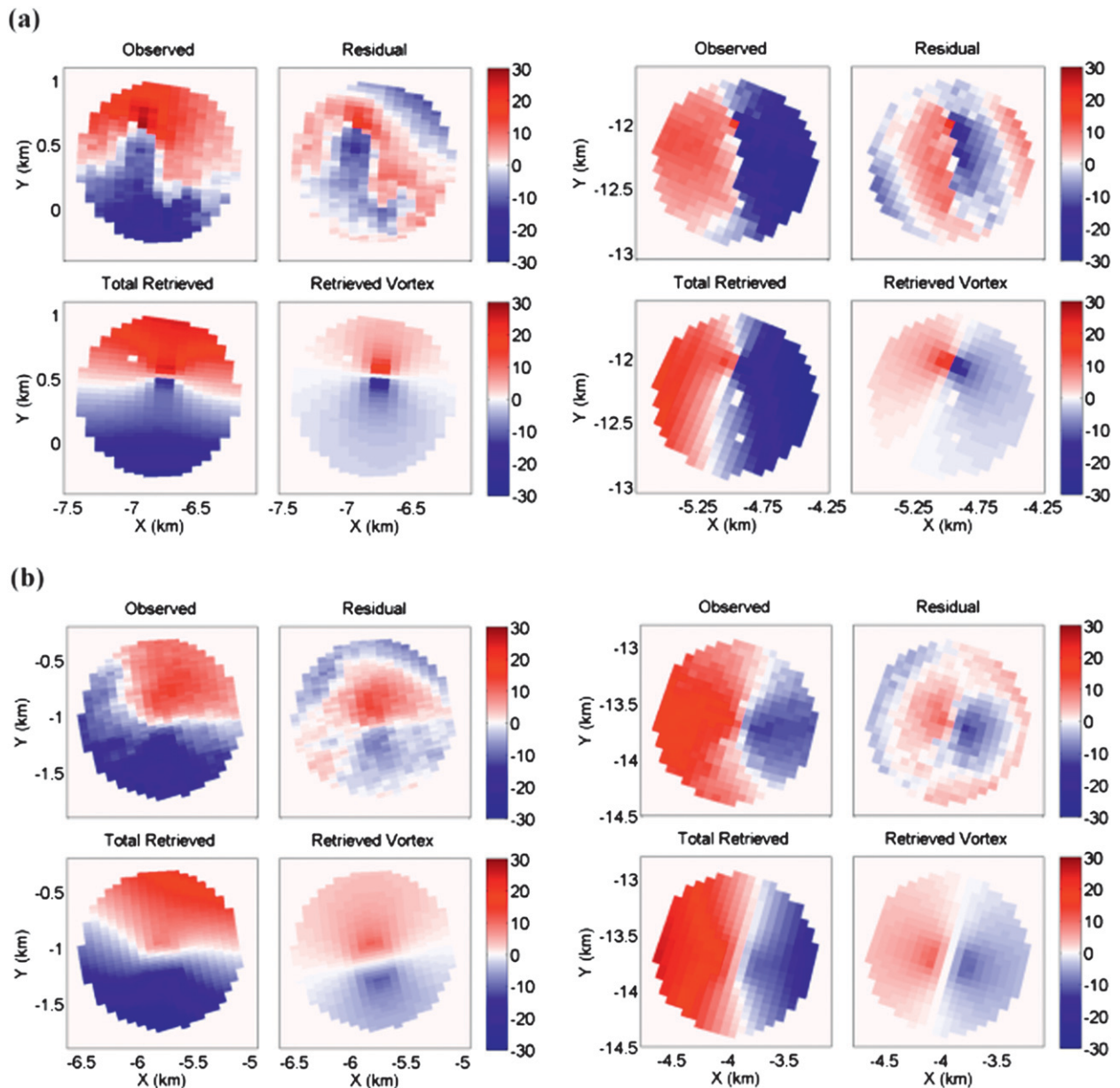


FIG. 6. Observed, residual (observed minus retrieved broad-scale), retrieved vortex, and retrieved total radial velocity fields for DOW radars located (left) east and (right) north-northeast of the analysis domain at (a) 0028 and (b) 0031 UTC. The axes indicate x and y displacements from the radar.

the radial wind speed and reflectivity exceed 15 m s^{-1} and 20 dBZ (respectively) in at least one radar gate within 3 km of the gate pair centroid. These criteria worked well at all five analysis times. All of the small-scale vortices evident within the mesoscale circulation were contained within one or more of the identified regions, and the numbers of identified regions were not prohibitively high, varying between 4 and 12 per analysis time.

Since forecasters must synthesize large amounts of information during severe weather operations, it may be

prudent to have the algorithm output mean vortex characteristic estimates from each set of detections likely corresponding to the same vortex (e.g., located within 500 m of one another) rather than from every retrieval. Thus, the ensemble (calculated over all retrievals passing the detection criteria) means of the most important retrieved vortex characteristics were computed at each analysis time in these tests (Table 2). To evaluate how well the mean retrieved vortex characteristics represent the actual vortex in each case, the radial component of

TABLE 4. Means of retrieved tornado characteristics for selected sets of 5 Jun 2001 retrievals from DOW radar data. Sample sizes appear in parentheses.

Time (UTC)	Distance from ensemble mean vortex center (m)	Movement speed (m s^{-1})	Heading ($0^\circ = \text{east}$)	V_T (m s^{-1})	V_T^{res} (m s^{-1})	V_R (m s^{-1})	R (m)	R_{10} (m)	α
0028 (5)	34	10	-64	26	10	3	66	167	1.0
0031 (7)	34	11	-67	12	11	0	165	216	0.8
0032 (16)	15	13	2	35	18	0	76	320	0.9

the final (not provisional) retrieval most closely approximating the ensemble mean retrieval for each analysis time was plotted and compared to the observed radial velocity field (the 0027 and 0033 UTC retrievals are shown in Fig. 5). In all five cases, the broad-scale portion of the model, though linear, recovered the larger-scale (parent vortex) circulation sufficiently well that the embedded vortices were salient in the residual flow. The embedded vortices were subsequently accurately retrieved on observed scales.

Significant differences occasionally occurred between the observed and retrieved radial wind fields over portions of the analysis domain. These discrepancies result from violations of the relatively simple low-order model. To the extent that these differences occur away from the stronger retrieved vortex flow, however, they do not seriously undermine the vortex retrieval. For example, the SR1-relative radial component of the total retrieved wind field is too strong in the northeastern part of the domain, but is reasonably similar to the SR1 radial wind field within the primary vortex circulation (Fig. 5a, left panel).

Although the “true” values of R_{20} , V_T , and other vortex characteristics cannot be precisely determined (and will not even be well defined in some cases, such as elliptical vortices), the retrieved values of these parameters can be qualitatively evaluated through comparison of the retrieved and observed wind fields in and near the retrieved vortex. In all five cases, the observed and mean retrieved radial velocity fields are in reasonable agreement, as are the radial components of the residual and retrieved vortex velocity fields. The mean R_{20} and V_T^{res} are largest for the 0033 and 0052 UTC analyses, consistent with the vortices at these times being larger and containing stronger maximum observed radial winds. In addition, the retrievals capture the strong convergence indicated in

the Doppler wind fields at 0022 UTC (observed wind field for this time not shown) and 0033 UTC (most evident at $x = -33$ km, $y = 24$ km in Fig. 5b).

The standard deviations in the retrieved vortex characteristics were calculated to quantify the uncertainty in these estimates (Table 3). While the uncertainty in the retrieved vortex center is small at each analysis time, the uncertainty in the vortex translational velocity is significant in some cases. This is not surprising since the vortices did not move very far during the 25–30-s retrieval periods (see section 3d). The uncertainty in the vortex model parameters V_T , α , and R tends to be higher than in the characteristics derived from them (e.g., R_{20} and V_T^{res}), indicating that the approach used to address the vortex solution nonuniqueness problem (section 4) worked well in these tests.

6. Experiments with DOW radar observations of a tornado

a. Description of dataset

The technique was next applied to a dual-DOW dataset of a tornado that occurred near Argonia, Kansas, on 5 June 2001 (Marquis et al. 2011). The intensity of the tornado is uncertain since no damage survey was performed; however, the maximum difference between the two peaks in the radial velocity couplet did not exceed ~ 50 m s^{-1} for either radar at any of the times considered here, suggesting that the tornado was relatively weak. The precise time period(s) during which the tornado occurred is unknown since its small size (~ 100 -m diameter; <http://www4.ncdc.noaa.gov/cgi-win/wwcgl.dll?wvent~ShowEvent~424514>) and probable low intensity as well as the presence of intervening precipitation prevented visual observation by the DOW team. The azimuthal sampling interval for both DOW radars averaged less

TABLE 5. Standard deviations of retrieved tornado characteristics for selected sets of 5 Jun 2001 retrievals from DOW radar data. Sample sizes appear in parentheses.

Time (UTC)	Distance from ensemble mean vortex center (m)	Movement speed (m s^{-1})	Heading ($0^\circ = \text{east}$)	V_T (m s^{-1})	V_T^{res} (m s^{-1})	V_R (m s^{-1})	R (m)	R_{10} (m)	α
0028 (5)	18	1	3	3	0	4	14	12	0.1
0031 (7)	16	4	31	1	2	1	14	54	0.1
0032 (16)	15	6	22	3	3	1	19	68	0.1

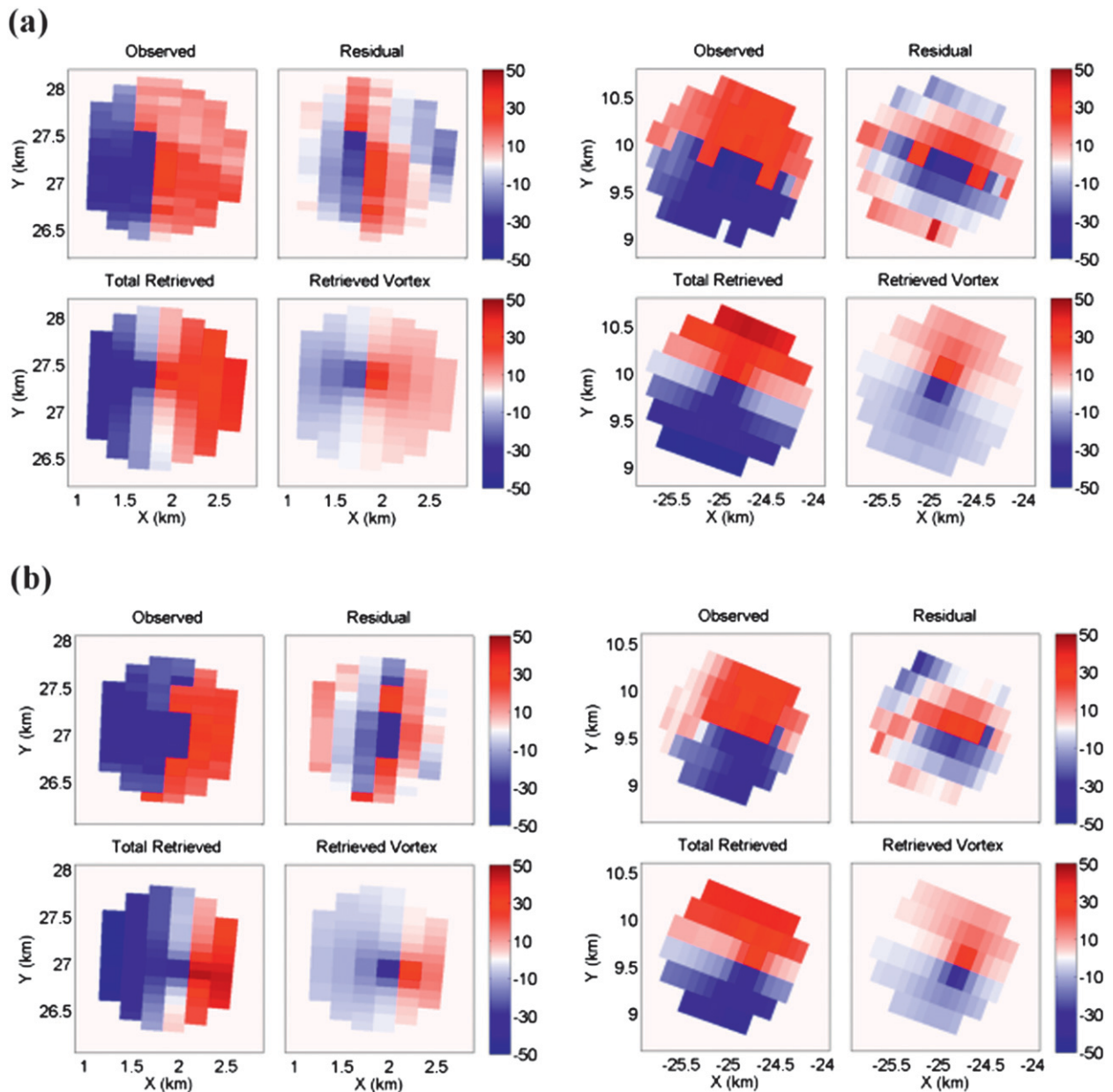


FIG. 7. Observed, residual (observed minus retrieved broad-scale), retrieved vortex, and retrieved total radial velocity fields for (left) KCYR and (right) KSAO at (a) 0233 and (b) 0234 UTC. The axes indicate x and y displacements from the radar.

than 0.4° and the radial sampling interval varied between 50 and 75 m. The azimuthal distance between observations near the tornado averaged around 50 m. Both radars had a 0.93° half-power beamwidth.

The radial velocity fields were dealiased and noisy or suspect reflectivity and velocity data were manually removed. An algorithm corrected for misalignment of successive sector scans (“jitter”). Given the relatively high quality of the raw radar data (D. Dowell 2010, personal communication) and the thoroughness of the quality

control, the radial velocity observations are likely reasonably representative of the actual wind field. The technique was applied to a single pair of PPI scans for seven consecutive coordinated volume scan pairs performed between 0028 and 0035 UTC. Each pair of PPI scans was selected such that the heights of the radar beams (typically ~ 100 – 150 m AGL) were within 100 m of each other near the tornado. In all cases, the radars observed the circulation within 5–15 s of one another.

TABLE 6. Mean retrieved tornado characteristics for three sets of 14 May 2009 retrievals from CASA IP-1 data. Sample sizes appear in parentheses.

Time (UTC)	Distance from ensemble mean vortex center (m)	Movement speed (m s^{-1})	Heading ($0^\circ = \text{east}$)	V_T (m s^{-1})	V_T^{res} (m s^{-1})	V_R (m s^{-1})	R (m)	R_{10} (m)	R_{30} (m)	α
0232 (8)	85	15	20	36	28	-17	123	419	172	1.0
0233 (15)	31	11	3	38	28	0	130	616	171	0.9
0234 (3)	26	11	-52	33	27	-2	138	555	153	0.9

b. Retrieval results

The same domain-selection criteria used in the 30 May 2004 experiments were used here, but with the additional requirement that gate-to-gate shear exceed 0.05 s^{-1} . Without this criterion, the number of identified radar gate pairs would have been much larger, primarily because of the very high observational resolution. The resulting additional processing would be highly undesirable during real-time operations. Retrievals were performed within two to six regions for each time period except 0032 UTC, for which 13 regions were selected for retrievals.

The detection threshold V_{det} was set to 10 m s^{-1} in these experiments, which is half that used in the 30 May 2004 experiments (as with the domain-selection criteria, the optimal value of V_{det} depends on the radar network and the types of vortices being sought). Fortunately, the technique detected the smallest intense vortex that could be subjectively inferred from the observed radial velocity fields at each of the analysis times. In several instances, the algorithm performed retrievals within regions that, based on visual examination of the radial velocity observations, contained strong shear but no intense vortices. However, no vortices with $V_T^{\text{res}} \geq 10 \text{ m s}^{-1}$ were identified other than those evident in the radar data.

Comparisons of the observed and final retrieved radial wind fields for selected time periods are presented in Fig. 6. Two separate small-scale vortices are apparent at 0028 UTC. The more northern vortex is the (possibly developing) tornado. Fortunately, both vortices were detected by the technique (retrievals of the nontornadic vortex not shown). The use of a modifiable (in particular, shrinkable) domain in steps 3 and 4 of the retrieval

procedure was critical to detecting the tornado in some cases. This is because the residual wind field at the end of step 1 was often dominated by a circulation intermediate in size between the tornado and the circulation retrieved (and subtracted) by the broad-scale model parameters.

The retrieved values of and trends in V_T^{res} , R_n , V_T , and R are consistent with the observed radial wind fields (Table 4). That the technique was able not only to detect but also to reasonably characterize this tornado is especially encouraging given its relatively small size and weak intensity. As in the 30 May 2004 experiments, there is little spread in the retrieved vortex center V_T^{res} and R_n among the detections for each period (Table 5). Because of the very high resolution afforded by the DOWs, the vortices are better resolved and so there is also less variance in V_T and R .

Despite the very short periods between scans used in each experiment, the (u_v, v_v) parameters were retrieved reasonably well (based on visual estimation of the vortex center at consecutive times) when the retrieved vortex had $R < 100 \text{ m}$. Consistent with the 30 May 2004 experiments, however, the variance in (u_v, v_v) increased when a larger vortex was detected due to the increased uncertainty in the vortex center. However, since the larger vortices retrieved in these experiments were relatively well resolved, the difficulty in retrieving their precise locations may be more attributable to the complexity of the wind field than to the finite observational resolution.

The (u_v, v_v) retrievals from these and the 30 May 2004 experiments suggest it may generally be more prudent to calculate the vortex translational velocity from the retrieved vortex centers at two consecutive times than to rely upon the retrieved (u_v, v_v) parameters. However, it

TABLE 7. Standard deviations of retrieved tornado characteristics for three sets of 14 May 2009 retrievals from CASA IP-1 data. Sample sizes appear in parentheses.

Time (UTC)	Distance from ensemble mean vortex center (m)	Movement speed (m s^{-1})	Heading ($0^\circ = \text{east}$)	V_T (m s^{-1})	V_T^{res} (m s^{-1})	V_R (m s^{-1})	R (m)	R_{10} (m)	R_{30} (m)	α
0232 (8)	35	2	10	15	5	6	33	140	35	0.2
0233 (15)	17	1	10	1	3	1	8	59	13	0.0
0234 (3)	16	2	15	3	3	1	19	22	11	0.0

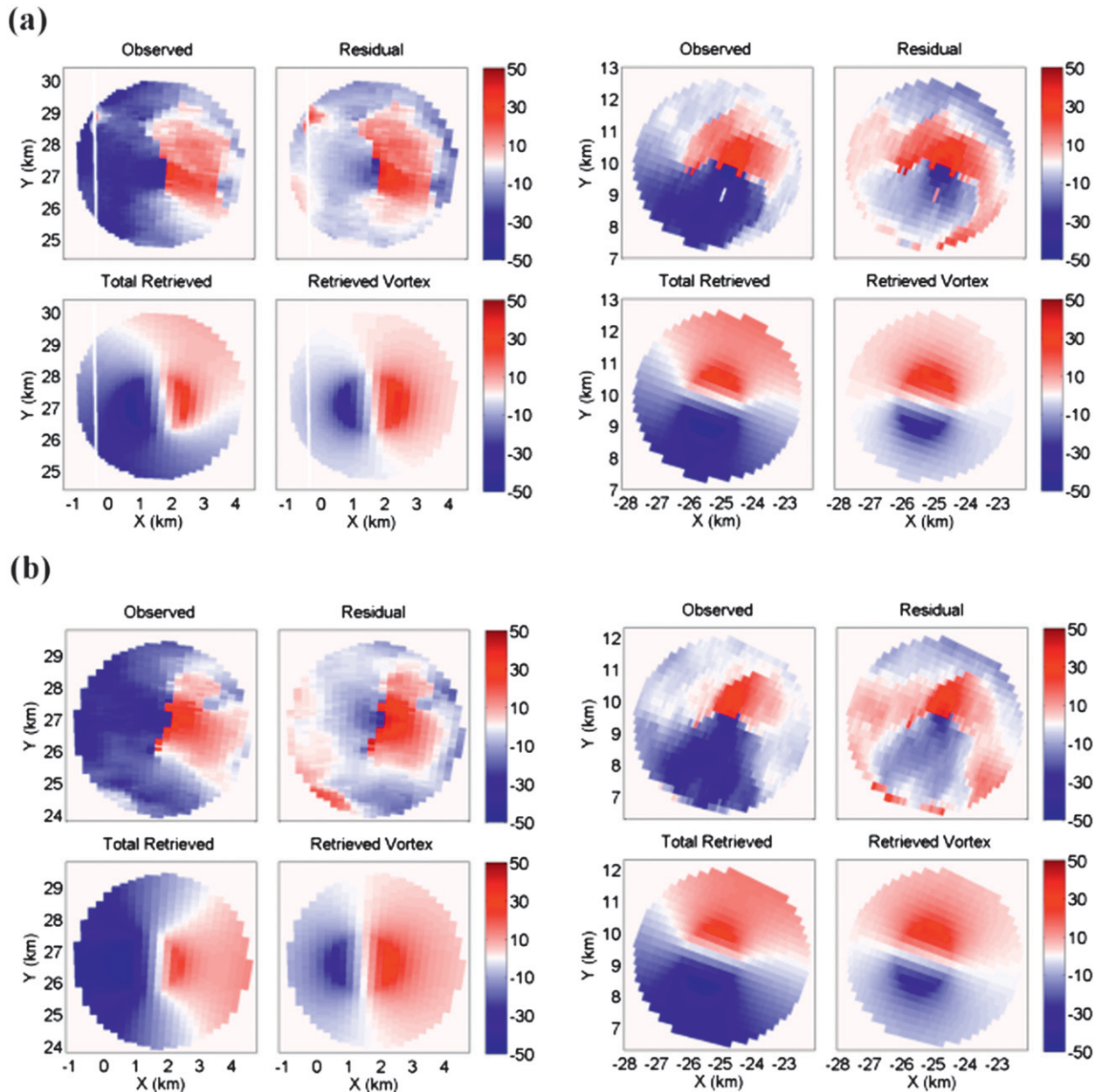


FIG. 8. As in Fig. 7, but for mesocyclone-mode retrievals.

does not follow that these parameters should be removed from the low-order model. If u_v and v_v are excluded from the retrieval procedure, then in cases where the vortex traverses a relatively large distance during the retrieval period, the vortex will be associated with two distinct minima in $J(x_0, y_0)$: one for the vortex location at the time of the first radar scan and one for the vortex location at the time of the second radar scan. In effect, the vortex will be treated by the technique as two separate stationary vortices or regions of linear shear (this is the converse of the problem discussed in section 3d in

which inaccurate retrieval of the vortex translational velocity can lead to two vortices or shear zones being erroneously treated as a single vortex). Since only one radar will contribute velocity data valid near the true vortex location to each minimum, the probability of detection will be reduced. Furthermore, in cases where the vortex is detected, substantial errors will occur in the retrieved vortex center if the observations primarily contributing to the vortex retrieval were collected by the later radar scan (since x_0 and y_0 are valid at the beginning of the retrieval period).

TABLE 8. Mean retrieved mesocyclone characteristics for three sets of 14 May 2009 mesocyclone-mode retrievals from CASA IP-1 data. Sample sizes appear in parentheses.

Time (UTC)	Distance from ensemble mean vortex center (m)	V_T (m s ⁻¹)	V_T^{res} (m s ⁻¹)	V_R (m s ⁻¹)	R (m)	R_{20} (m)	α
0232 (4)	117	36	31	-4	953	1360	1.7
0233 (6)	99	40	26	7	813	1098	2.2
0234 (7)	93	38	28	3	947	1428	1.6

To confirm this reasoning, experiments with and without u_v and v_v were performed using the 0031:31 UTC scan from the DOW radar located east of the analysis and the 0032:38 UTC scan from the DOW radar located north-northeast of the domain. Retrievals (not shown) were performed over a single set of analysis domains centered on the true tornado location. Using the original low-order model, the tornado was detected in seven out of nine retrievals, and the u_v and v_v were well retrieved because of the large distance (~ 1 km) traveled by the tornado between the times of the two radar scans. Removing u_v and v_v from the low-order model, however, reduced the number of successful detections to two and increased the error in the mean retrieved vortex location by ~ 500 m. It is thus recommended that u_v and v_v be included in the low-order model unless the periods between the radar scans used in the retrievals are so short that even rapidly translating vortices are unlikely to move very far (relative to the observational resolution) during the retrieval period.

7. CASA observations of the 14 May 2009 Anadarko, Oklahoma, tornado

a. Description of dataset

An EF-2 tornado that impacted Anadarko, Oklahoma, from 0226 to 0244 UTC 14 May 2009 was sampled by two CASA Integrated Project 1 (IP-1; Brotzge et al. 2010; Junyent et al. 2010) radars. The technique was tested using the 2° PPI scans from the 0232, 0233, and 0234 UTC KCYR and KSAO volume scans, yielding an analysis domain height of ~ 1 km at the tornado, which was located 25–30 km from both radars. The velocity data were

manually dealiased and objectively filtered. The radars sampled every 96 m in range and 0.5° in azimuth and have a 1.8° half-power beamwidth. The radars observed the tornado within 4, 13, and 8 s of each other at 0232, 0233, and 0234 UTC, respectively.

Unfortunately, the high density of spurious data in/near the tornado in the raw radial velocity fields makes the representativeness of the edited velocity fields uncertain. However, the edited velocity fields appear reasonably representative of a strong tornado, regardless of how accurately they represent this particular tornado. This is therefore a valuable (albeit nonideal) test case for the technique.

b. Retrieval results

These experiments used the same domain-selection criteria and V_{det} value (10 m s^{-1}) as the 5 June 2001 experiments. Retrievals were performed in 15, 13, and 3 regions at 0232, 0233, and 0234 UTC, respectively. Verification of the retrieved vortex characteristics in this case is somewhat hindered by the difficulty in visually distinguishing between the tornado and the mesocyclonic flow in the velocity observations (Fig. 7). However, the technique does detect the tornado at each time, and the retrieved vortex locations and translation velocities (Table 6) are roughly consistent with the velocity observations. In addition, the retrieved R_{30} at each time is broadly consistent with the surveyed 250-yd (228.6 m) damage path width (<http://www4.ncdc.noaa.gov/cgi-win/wwcgi.dll?wwevent~ShowEvent~761954>), and the standard deviations in the retrieved vortex characteristics are relatively small (Table 7). The V_T^{res} is significantly lower than the maximum winds that actually occurred in the tornado.

TABLE 9. Mean retrieved vortex characteristics for five sets of 30 May 2004 mesocyclone-mode retrievals from SMART-Radar data. Sample sizes appear in parentheses.

Time (UTC)	Distance from ensemble mean vortex center (m)	V_T (m s ⁻¹)	V_T^{res} (m s ⁻¹)	V_R (m s ⁻¹)	R (m)	R_{20} (m)	R_{30} (m)	R_{40} (m)	R_{50} (m)	α
0022 (3)	154	35	25	-13	1281	1929	—	—	—	1.6
0027 (9)	137	38	25	-3	1039	1624	—	—	—	1.6
0033 (13)	168	45	35	-18	920	1637	1242	—	—	1.5
0038 (14)	190	51	29	-7	1161	2067	1691	—	—	1.7
0052 (10)	109	70	50	-2	894	2360	1721	1376	1156	1.3

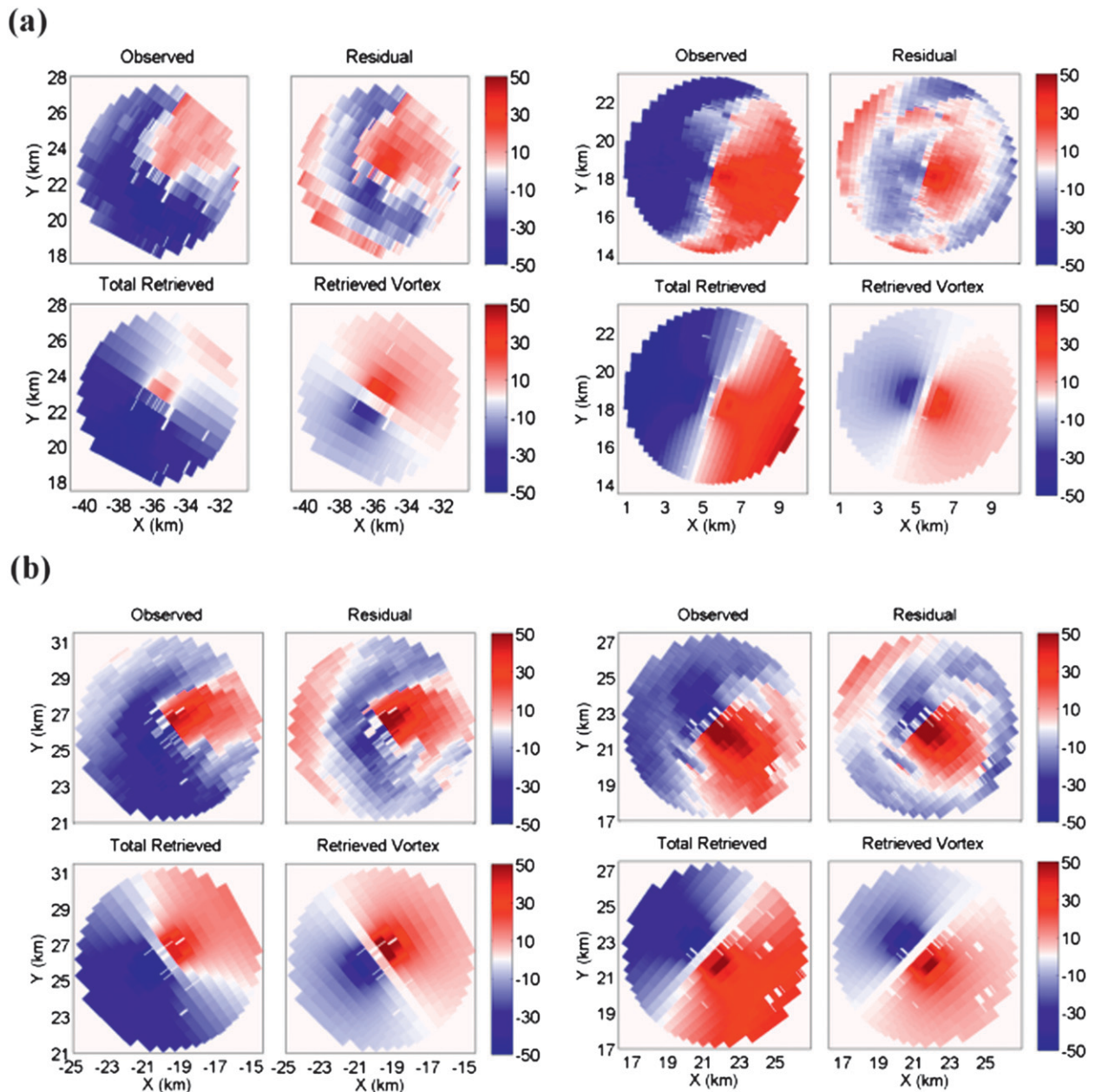


FIG. 9. As in Fig. 5, but for mesocyclone-mode retrievals at (a) 0027 and (b) 0052 UTC.

This is not surprising since the azimuthal sampling interval and beamwidth for both radars were ~ 250 m and ~ 1 km (respectively) at the range of the tornado, while the tornado core diameter was presumably < 250 m (i.e., narrower than the reported damage path). Nevertheless, the retrieved V_T^{res} and R_{30} indicate a tornado-like vortex, an encouraging result given the indistinctness of the tornado in the observed radial wind fields. The rapid change in V_R between 0032 and 0033 UTC seems physically unrealistic and is not supported by the observed radial wind fields (not

shown for 0032 UTC). The suitability of the vortex radial wind profile in our low-order model is briefly discussed in section 8.

In addition to the tornado, several weaker vortices (not shown) were retrieved in other regions of the dual-Doppler domain. In agreement with the observations, these vortices were significantly less intense than the retrieved tornado ($V_T^{\text{res}} = 10 \text{ m s}^{-1}$ in all cases) and thus would not have unduly diverted forecasters' attention.

TABLE 10. As in Table 9, but for retrievals using data from SR1 only. Sample sizes appear in parentheses.

Time (UTC)	Distance from dual-Doppler vortex center (m)	V_T (m s ⁻¹)	V_T^{res} (m s ⁻¹)	V_R (m s ⁻¹)	R (m)	R_{20} (m)	α
0022 (1)	282	40	25	-13	1170	2495	0.9
0027 (2)	218	36	20	-4	949	1555	1.2
0033 (8)	127	38	27	-21	945	1694	1.2
0038 (8)	341	49	23	1	1324	2168	1.9
0052 (7)	700	59	25	2	964	2830	1.0

8. Retrieving larger-scale vortices

a. Mesocyclone retrieval configuration

Upon verifying the technique's ability to detect and characterize vortices ≤ 1 km in diameter, the technique was next applied to larger-scale vortices. Since supercells produce much of the significant severe weather in the United States, timely detection of mesocyclones is critical to severe weather operations. Although mesocyclones already tend to be quickly detected during severe weather operations (either by objective algorithms or through visual inspection of radial velocity data), the vortex size and strength estimates provided by the VDAC technique may provide valuable additional guidance to forecasters. In addition, the diameters of the largest tornadoes and of mesovortices embedded in mesoscale convective systems can exceed 1 km.

To facilitate the retrieval of larger vortices, the algorithm was modified to include a user-selectable "mesocyclone mode" tailored to the retrieval of vortices ~ 1 –6 km in diameter. Ideally, this version of the technique would run concurrently with the original version. The first guess R is set to 1 km (rather than 200 m) in the mesocyclone retrieval configuration, and the x and y spacing between vortex center first guesses is 1500 m (rather than 500 m). The initial analysis domain radius is set to 5 km (rather than 2 km), and the analysis domain in steps 3 and 4 of the retrieval procedure is sized such that the vortex radius of $V_T/3$ or 10 m s^{-1} winds (whichever is larger) borders the edge of the domain at the end of the retrieval period. As in the original retrieval configuration, the modified analysis domain radius is not allowed to exceed that of the initial analysis domain. The

V_{det} threshold is set to 20 m s^{-1} (rather than 10 m s^{-1}) since the stronger winds associated with the vortex core are more likely to be observed in larger vortices. In addition, the rms error in each radar's retrieved radial wind within R_{det} of the vortex center (section 4) must be less than 75% (rather than 100%) of the rms observed radial wind over the same region for a detection to be made. This last modification was motivated by a few relatively poor vortex retrievals in preliminary experiments.

b. Dual-Doppler experiments

The 14 May 2009 and 30 May 2004 experiments were repeated using the mesocyclone retrieval configuration described above. As in the original experiments, the collocation of different-sized vortices posed a significant challenge to the technique. In the new experiments, however, the target vortices themselves contained smaller-scale vortices. Since vortices that are significantly smaller than the analysis domain are not captured by the broad-scale model parameters and thus are not subtracted from the observed radial wind field before the vortex retrieval, one concern was that the retrieved vortices in these experiments would be more representative of the sum of the two vortex wind fields than of the larger vortex alone.

Fortunately, the 14 May 2009 mesocyclone was detected at all three times, and no false detections were made. Visual comparisons of the residual and retrieved vortex wind fields (Fig. 8) indicate that the presence of the tornado had little impact on the retrievals of the larger-scale vortex. The mesocyclone is evidently sufficiently dominant in the wind field that minima in J

TABLE 11. As in Table 9, but for retrievals using data from SR2 only. Sample sizes appear in parentheses.

Time (UTC)	Distance from dual-Doppler vortex center (m)	V_T (m s ⁻¹)	V_T^{res} (m s ⁻¹)	V_R (m s ⁻¹)	R (m)	R_{20} (m)	α
0022 (0)	N/A	N/A	N/A	N/A	N/A	N/A	N/A
0027 (3)	203	44	20	4	910	2308	1.0
0033 (6)	1357	55	30	-7	989	2731	1.2
0038 (8)	1317	53	20	3	1221	3824	0.9
0052 (4)	243	75	34	1	911	2802	1.2

primarily associated with the tornado are unlikely to be reached from a given first-guess vortex center. The mean retrieved R , R_{20} , and V_T^{res} (Table 8) all appear consistent with the observed wind fields.

The results of the 30 May 2004 mesocyclone-mode experiments were similarly encouraging. The larger-scale (1–2 km in diameter) vortex was detected at all five times with no false detections made. The mean V_T^{res} and R_{20} (Table 9) successfully captured the expansion of the stronger vortex winds with time (Fig. 9). Consistent with the surveyed damage, the technique detected F-2 (50–69 m s^{-1} ; Fujita 1981) vortex winds at 0052 UTC.

A 5-km radius analysis domain is not wide enough to encompass larger mesocyclones, the diameters of which can reach ~ 10 km. Therefore, a third retrieval configuration using an initial analysis domain radius of 10 km and first-guess R of 3 km was preliminarily tested using the 30 May 2004 case. Fortunately, retrievals of the mesocyclone (diameter $\approx 6+$ km) surrounding the vortices retrieved in sections 5b and 8b showed reasonable qualitative agreement with the observed radial wind fields at all five retrieval times. However, since smaller-scale vortices are the focus of this study, these results are not shown.

c. Single-Doppler experiments

Having validated the mesocyclone retrieval configuration, the ability of the technique to detect and characterize vortices ~ 1 km in radius in cases where only single-Doppler data are available was assessed. To do this, the retrievals in section 8b were repeated but using data only from a single radar (e.g., KCYR and KSAO, in turn).

The 30 May 2004 circulation was detected at all five times using the SR1 data and at four of the five times using the SR2 data (Tables 10 and 11). The failure of the 0022 UTC SR2-only retrievals to detect the mesocyclone is likely due in part to the highly complex radial wind field present at this time (not shown). The vortex parameter values retrieved in the single-Doppler experiments were generally comparable to those retrieved in the dual-Doppler experiments. A notable exception was the frequently substantial differences in V_R between the single-Doppler (particularly the SR2-only) experiments and the dual-Doppler experiments. These discrepancies as well as those which occurred in the 13 May 2009 tornado retrievals (section 7) and mesocyclone-mode experiments (see below) suggest that the MCRV model of the vortex radial wind component may often be inappropriate for real convective vortices. One potentially valuable focus of future work would be to test

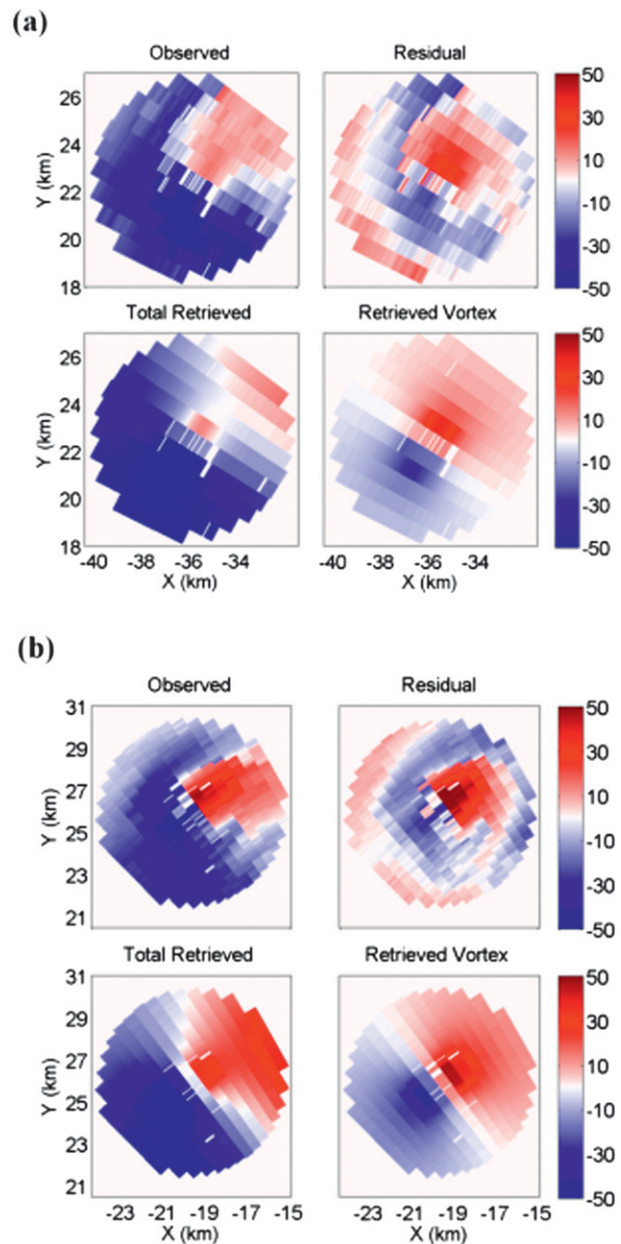


FIG. 10. As in Fig. 9, but for retrievals using data from SR1 only.

a modified version of the low-order model in which the radii of the maximum vortex radial and tangential winds are controlled by separate parameters.

Despite the large discrepancies in V_R , the retrieved wind fields in the single-Doppler experiments were in reasonable agreement with the observations (Fig. 10). The mean retrieved V_T^{res} was significantly lower in both the SR2 and (especially) the SR1 0052 UTC experiments, despite mean V_T values that were similar to those retrieved in the dual-Doppler 0052 UTC experiment. This is because the angular separation criterion

TABLE 12. As in Table 8 except for retrievals using only data from KCYR.

Time (UTC)	Distance from dual-Doppler vortex center (m)	V_T (m s^{-1})	V_T^{res} (m s^{-1})	V_R (m s^{-1})	R (m)	R_{20} (m)	α
0232 (2)	215	27	23	-1	1193	1444	1.7
0233 (3)	1234	37	20	0	1327	2027	1.3
0234 (1)	76	48	20	-4	1179	1921	1.8

for a given V_T^{res} to be obtained (section 4) is much more difficult to satisfy when data are available from only one radar, particularly if vortex winds of that magnitude are not well resolved. The larger differences that occasionally occurred in the mean retrieved tornado center between the dual- and single-Doppler experiments are not surprising given the complexity of the wind field.

Fortunately, the 14 May 2009 mesocyclone was detected in all of the single-Doppler experiments, and no false detections were made (Tables 12 and 13; Fig. 11). As in the 30 May 2004 experiments, the V_T^{res} values were generally lower for the single-Doppler retrievals, and V_R was highly sensitive to which radar(s) contributed data to the retrieval. The R and V_R in the dual-Doppler experiments appear to split the difference between the two sets of single-Doppler experiments, suggesting that both radars contributed useful velocity information to the dual-Doppler retrievals. This makes sense given that the two radars were roughly equidistant from the mesocyclone.

9. Summary and conclusions

Two major improvements have been made to the original VDAC technique described in Potvin et al. (2009). First, the retrieval procedure has been extended to allow the analysis domain to be relocated and resized based on a preliminary vortex retrieval. This allows the analysis domain to be made as small as possible (without truncating too much of the outer vortex flow), thereby making the vortex more dominant in the wind field. Second, the detection criteria have been redesigned to determine whether retrieved vortex characteristics are consistent with the observed wind field. Such a “reality check” is critical because of the existence

of multiple minima in the cost function, especially those associated with nonuniqueness in the MCRV model parameters.

Tests with real Doppler observations of intense vortices indicate the VDAC technique is capable of detecting and characterizing vortices reasonably well, even when they are embedded within a complex wind field or a larger, stronger vortex. The vortex characteristic estimates output by the technique could help forecasters to triage storms during severe weather outbreaks, thus facilitating timely identification of tornadoes, mesocyclones, and other significant convective vortices.

No false detections were made in any of our experiments, despite our use of nonrestrictive domain-selection and vortex detection criteria to minimize the risk of missed detections. Thus, computational considerations aside, the technique does not appear unduly sensitive to these criteria. Prior to real-time implementation, however, the computational expense of the technique (each set of nine retrievals in our CASA IP-1 experiments required 30–60 s on a single AMD 2.6-GHz Opteron processor) would need to be considered in optimizing the domain-selection criteria. Fortunately, the execution of the algorithm could be greatly accelerated by performing each set of retrievals on a different processor. The impact of velocity data artifacts (e.g., aliasing) characteristic of a given radar network would also need to be explored. However, the ability of the VDAC technique to simultaneously use velocity data from multiple radars and radar gates should render it less prone than conventional methods to making false detections in regions containing erroneous velocity values. The technique is capable of detecting and characterizing larger-scale vortices such as mesocyclones even when only single-Doppler data are available. It may therefore be useful to run the mesocyclone-retrieval configuration of the technique in

TABLE 13. As in Table 8 except for retrievals using only data from KSAO.

Time (UTC)	Distance from dual-Doppler vortex center (m)	V_T (m s^{-1})	V_T^{res} (m s^{-1})	V_R (m s^{-1})	R (m)	R_{20} (m)	α
0232 (8)	212	53	28	-7	570	1847	0.9
0233 (4)	328	48	28	10	681	1464	1.7
0234 (9)	423	46	21	8	843	1897	1.0

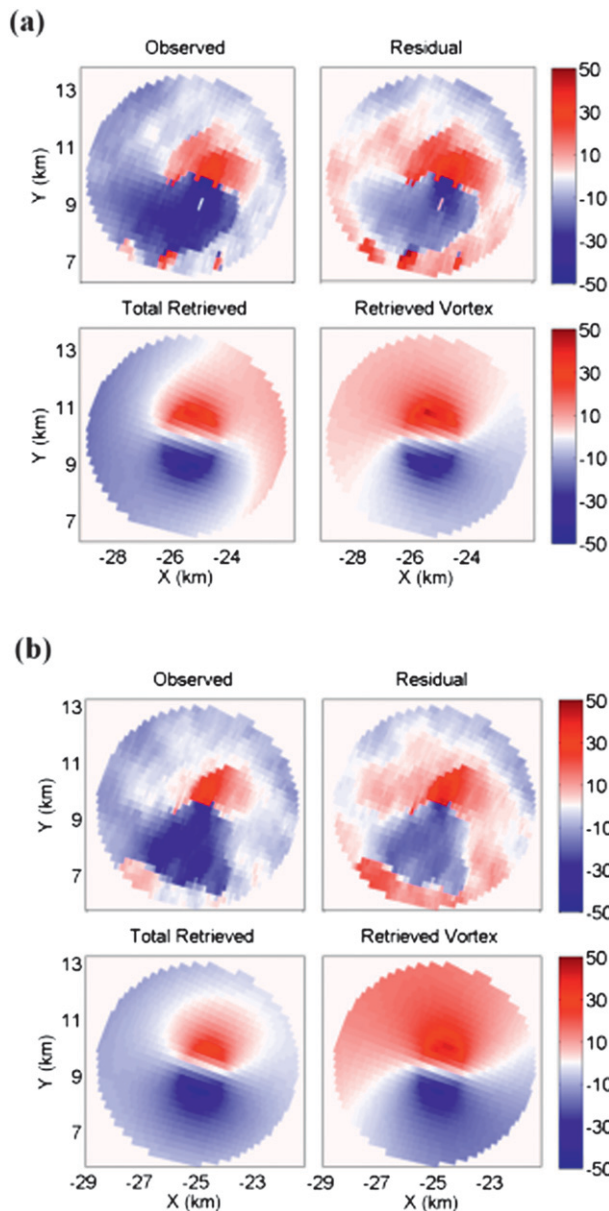


FIG. 11. As in Fig. 8, but for retrievals using data from KSAO only.

real time on WSR-88D data, at least for shorter radar ranges. This would greatly expand the domain over which the technique could be applied and could create useful data for vortex climatology studies. For example, correlating tornadogenesis potential to mesocyclone characteristics has been recognized as a worthwhile research endeavor, but one that requires an extensive climatology of mesocyclone characteristics (McGrath et al. 2002). This technique would provide an objective, possibly automated means of characterizing the sizes and strengths of tornadic and nontornadic mesocyclones.

Acknowledgments. This work was primarily supported by NSF Grant EEC-031347, through the Engineering Research Center (ERC) for Collaborative Adaptive Sensing of the Atmosphere (CASA). The CASA velocity data were edited by V. Chandrasekar and Nitin Bharadwaj. The SMART radar data were collected and provided by M. Biggerstaff and edited by K. Kuhlman and D. Betten under NSF Grants ATM-0619715 and ATM-0802717. The DOW data were edited by David Dowell. We appreciate the contributions of the DOW crew including Curtis Alexander, MyShelle Bryant, Bob Conzemius, David Dowell, Steve McDonald, Kevin McGrath, Kevin Scharfenberg, Herb Stein, Josh Wurman, and Pengfei Zhang during ROTATE (Radar Observations of Tornadoes and Thunderstorms Experiment) 2001. The DOW radars and their data were supported by NSF Grants ATM-0734001 and ATM-801041.

REFERENCES

- Biggerstaff, M. I., and Coauthors, 2005: The Shared Mobile Atmospheric Research and Teaching Radar: A collaboration to enhance research and teaching. *Bull. Amer. Meteor. Soc.*, **86**, 1263–1274.
- Bluestein, H. B., W.-C. Lee, M. Bell, C. C. Weiss, and A. L. Pazmany, 2003: Mobile Doppler radar observations of a tornado in a supercell near Bassett, Nebraska, on 5 June 1999. Part II: Tornado-vortex structure. *Mon. Wea. Rev.*, **131**, 2968–2984.
- , M. M. French, R. L. Tanamachi, S. Frasier, K. Hardwick, F. Junyent, and A. L. Pazmany, 2007: Close-range observations of tornadoes in supercells made with a dual-polarization, X-band, mobile Doppler radar. *Mon. Wea. Rev.*, **135**, 1522–1543.
- Brotzge, J., and S. Erickson, 2010: Tornadoes without NWS warning. *Wea. Forecasting*, **25**, 159–172.
- , and Coauthors, 2007: CASA IP1: Network operations and initial data. *Extended Abstracts, 23rd Conf. on Interactive Information and Processing Systems*, San Antonio, TX, Amer. Meteor. Soc., 8A.6. [Available online at http://ams.confex.com/ams/87ANNUAL/techprogram/paper_120056.htm.]
- , K. Hondl, B. Philips, L. Lemon, E. J. Bass, D. Rude, and D. L. Andra, 2010: Evaluation of distributed collaborative adaptive sensing for detection of low-level circulations and implications for severe weather warning operations. *Wea. Forecasting*, **25**, 173–189.
- Brown, R. A., V. T. Wood, and D. Sirmans, 2002: Improved tornado detection using simulated and actual WSR-88D data with enhanced resolution. *J. Atmos. Oceanic Technol.*, **19**, 1759–1771.
- Center for Severe Weather Research, cited 2010: Preliminary radar analysis of the Geary-Calumet, Oklahoma tornadoes occurring on 29 May 2004. [Available online at <http://www.cswr.org/dataimages/rotate/geary-summary-2004-0711fp.pdf>.]
- Crum, T. D., and R. L. Alberty, 1993: The WSR-88D and the WSR-88D Operational Support Facility. *Bull. Amer. Meteor. Soc.*, **74**, 1669–1687.
- Fletcher, R., and C. M. Reeves, 1964: Function minimization by conjugate gradients. *Comput. J.*, **7**, 149–153.
- Fujita, T. T., 1981: Tornadoes and downbursts in the context of generalized planetary scales. *J. Atmos. Sci.*, **38**, 1511–1534.

- Gal-Chen, T., 1982: Errors in fixed and moving frames of reference: applications for conventional and Doppler radar analysis. *J. Atmos. Sci.*, **39**, 2279–2300.
- Hughes, L. A., 1952: On the low-level wind structure of tropical storms. *J. Meteor.*, **9**, 422–428.
- Junyent, F., V. Chandrasekar, D. McLaughlin, E. Insanic, and N. Bharadwaj, 2010: The CASA Integrated Project 1 networked radar system. *J. Atmos. Oceanic Technol.*, **27**, 61–78.
- Kuhlman, K. M., D. R. MacGorman, M. I. Biggerstaff, and P. R. Krehbiel, 2009: Lightning initiation in the anvils of two supercell storms. *Geophys. Res. Lett.*, **36**, L07802, doi:10.1029/2008GL036650.
- Lee, W.-C., and J. Wurman, 2005: Diagnosed three-dimensional axisymmetric structure of the Mulhall tornado on 3 May 1999. *J. Atmos. Sci.*, **62**, 2373–2393.
- , F. D. Marks Jr., and R. E. Carbone, 1994: Velocity track display—A technique to extract real-time tropical cyclone circulations using a single airborne Doppler radar. *J. Atmos. Oceanic Technol.*, **11**, 337–356.
- , B. J.-D. Jou, P.-L. Chang, and S.-M. Deng, 1999: Tropical cyclone kinematic structure retrieved from single-Doppler radar observations. Part I: Interpretation of Doppler velocity patterns and the GBVTD technique. *Mon. Wea. Rev.*, **127**, 2419–2439.
- Lewellen, D. C., W. S. Lewellen, and J. Xia, 2000: The influence of a local swirl ratio on tornado intensification near the surface. *J. Atmos. Sci.*, **57**, 527–544.
- Liou, Y.-C., T.-C. Chen Wang, W.-C. Lee, and Y.-J. Chang, 2006: The retrieval of asymmetric tropical cyclone structures using Doppler radar simulations and observations with the extended GBVTD technique. *Mon. Wea. Rev.*, **134**, 1140–1160.
- MacGorman, D. R., and Coauthors, 2008: TELEX: The Thunderstorm Electrification and Lightning Experiment. *Bull. Amer. Meteor. Soc.*, **89**, 997–1013.
- Marquis, J., Y. Richardson, P. Markowski, D. Dowell, and J. Wurman, 2011: Tornado maintenance investigated with high-resolution dual-Doppler and EnKF analysis. *Mon. Wea. Rev.*, in press.
- McGrath, K. M., T. A. Jones, and J. T. Snow, 2002: Increasing the usefulness of a mesocyclone climatology. Preprints, *21st Conf. on Severe Local Storms*, San Antonio, TX, Amer. Meteor. Soc., 162–165.
- McLaughlin, D., and Coauthors, 2005: Distributed Collaborative Adaptive Sensing (DCAS) for improved detection, understanding, and predicting of atmospheric hazards. *Extended Abstracts, Ninth Symp. on Integrated Observing and Assimilation Systems for the Atmosphere, Oceans, and Land Surface*, San Diego, CA, Amer. Meteor. Soc., 11.3. [Available online at http://ams.confex.com/ams/Annual2005/techprogram/paper_87890.htm.]
- Mitchell, E. D., S. V. Vasiloff, G. J. Stumpf, A. Witt, M. D. Eilts, J. T. Johnson, and K. W. Thomas, 1998: The National Severe Storms Laboratory tornado detection algorithm. *Wea. Forecasting*, **13**, 352–366.
- Payne, C. D., T. J. Schuur, D. R. MacGorman, M. I. Biggerstaff, K. Kuhlman, and W. D. Rust, 2010: Polarimetric and electrical characteristics of a lightning ring in a supercell storm. *Mon. Wea. Rev.*, **138**, 2405–2425.
- Polak, E., and G. Ribiere, 1969: Note sur la convergence de methods de directions conjuguées. *Rev. Franc. Informat. Rech. Operationnelle*, **16**, 35–43.
- Potvin, C. K., A. Shapiro, T. Y. Yu, J. Gao, and M. Xue, 2009: Using a low-order model to detect and characterize tornadoes in multiple-Doppler radar data. *Mon. Wea. Rev.*, **137**, 1230–1249.
- Roux, F., and F. D. Marks, 1996: Extended velocity track display (EVTD): An improved processing method for Doppler radar observation of tropical cyclones. *J. Atmos. Oceanic Technol.*, **13**, 875–899.
- Stumpf, J. G., A. Witt, E. D. Mitchell, P. L. Spencer, J. T. Johnson, M. D. Eilts, K. W. Thomas, and D. W. Burgess, 1998: The National Severe Storms Laboratory mesocyclone detection algorithm for the WSR-88D. *Wea. Forecasting*, **13**, 304–326.
- Wurman, J., 2002: The multiple-vortex structure of a tornado. *Wea. Forecasting*, **17**, 473–505.
- , and S. Gill, 2000: Finescale radar observations of the Dimmitt, Texas (2 June 1995), tornado. *Mon. Wea. Rev.*, **128**, 2135–2164.
- , J. Straka, E. Rasmussen, M. Randall, and A. Zahrai, 1997: Design and deployment of a portable, pencil-beam, pulsed, 3-cm Doppler radar. *J. Atmos. Oceanic Technol.*, **14**, 1502–1512.